Efficient modal-expansion discrete-dipole approximation: Application to the simulation of optical extinction and electron energy-loss spectroscopies

Stéphane-Olivier Guillaume,[1] F. Javier García de Abajo,[2,3] and Luc Henrard[1,*]
[1]*Department of Physics, University of Namur, rue de Bruxelles 61, B-5000 Namur, Belgium*
[2]*ICFO–Institut de Ciencies Fotoniques, Mediterranean Technology Park, 08860 Castelldefels (Barcelona), Spain*
[3]*ICREA–Institució Catalana de Recerca i Estudis Avançats, Barcelona, Spain*
(Received 4 October 2013; published 26 December 2013)

An efficient procedure is introduced for the calculation of the optical response of individual and coupled metallic nanoparticles in the framework of the discrete-dipole approximation (DDA). We introduce a modal expansion in the basis set of discrete dipoles and show that a few suitably selected modes are sufficient to compute optical spectra with reasonable accuracy, thus reducing the required numerical effort relative to other DDA approaches. Our method offers a natural framework for the study of localized plasmon modes, including plasmon hybridization. As a proof of concept, we investigate optical extinction and electron energy-loss spectra of monomers, dimers, and quadrumers formed by flat silver squares. This method should find application to the previously prohibited simulation of complex particle arrays.

DOI: 10.1103/PhysRevB.88.245439 PACS number(s): 78.67.Bf, 78.20.Bh, 79.20.Uv

I. INTRODUCTION

Metallic nanoparticles have been recognized as excellent tools to manipulate light at the nanoscale, enabling deep-subwavelength optical confinement and extreme electromagnetic field enhancement.[1] This has triggered a massive amount of work in search of applications to ultrasensitive molecular detection,[2,3] improved photovoltaics,[4] surface-enhanced spectroscopies,[5–7] and optical signal processing,[8,9] among other feats. The optical properties underlying these applications are associated with plasmons supported by the nanoparticles, which emerge as strong spectral features in the UV–near-infrared (UV–NIR) spectral range and consist of collective oscillations of valence electrons.[10] The frequency, width, and optical strength of plasmons are strongly dependent on the nanoparticle morphology, size, composition, and environment.[11–13] Particles of small size compared with the light wavelength are especially important, as they can support strong dipolar modes, whereas higher-order modes become relatively dark.

Aside from isolated nanoparticles, coupled systems such as dimers,[14] trimers,[15] and arrays of nanoparticles[16] have also been investigated and their plasmon modes found to be describable within a hybridization scheme of the modes of the individual nanoparticles.[17] This has revealed the existence of so-called *bright* and *dark* modes, depending on their ability to couple to light.[18] For example, when the plasmons of assembled small nanoparticles combine in such a way that the total dipole moment vanishes, the interaction with light is weak (actually, zero in the small-particle limit), thus producing no features in the optical spectra. An effective way of resolving such dark modes is by exciting them with a focused electron beam. The excited plasmons leave a trace in the electrons as specific energy losses, which can be measured by means of an electron microscope equipped with an electron spectrometer.[19,20] The small spatial extension of the electromagnetic field associated with a fast electron enables a local interaction with the nanoparticles, giving rise to the excitation of some plasmons, depending on the electron trajectory.[21] Alternatively, dark modes can also be excited by breaking the symmetry of the system, so that they become brighter, as demonstrated using nanorod dimers.[19,22] Incidentally, coupled systems are good candidates for sensing applications, using some of the properties of Fano resonances,[23–25] as recently shown by optical and electron energy-loss (EEL) experiments.[26,27]

In this work, we focus on the simulation of optical extinction and EEL spectra of isolated and coupled metallic particles as a proof of principle of our approach. Although several methods already exist for performing such calculations, they suffer from various drawbacks. For instance, the boundary element method (BEM) requires us to parametrize the boundaries between different materials[12,28] and this can be a complicated task for complex structures. Also, the finite difference in the time domain (FDTD) approach becomes very inefficient for large systems consisting of sparse distributions of materials (e.g., distant particles, narrow wires, etc.), as it relies on three-dimensional (3D) parametrization of space, including empty regions.[29,30] Multiple-scattering T-matrix techniques[31,32] are limited to simple particles (e.g., spheres) and have severe constraints regarding their arrangement (e.g., multipolar expansions converge very weakly for intertwined objects). In contrast, the discrete-dipole approximation[33,34] (DDA) is a volume method that is well adapted for describing complex shapes, including sparse systems, although the calculation time grows rapidly for systems consisting of many particles. Our goal here is to develop an efficient procedure to compute optical extinction and EEL spectra for clusters of arbitrarily shaped particles. We accomplish this task by using an eigenvector expansion of the physical quantities entering the DDA formalism, instead of directly solving the complete self-consistent coupled-dipoles equation. We find that this expansion can be truncated to a few terms compared with the complete basis set containing thousands of vectors, provided those terms are carefully chosen, as prescribed below. The response of the whole system is then obtained by adding interaction terms that account for multiple scattering between the particles. In this way, the numerical size of the problem is considerably reduced, particularly in large systems formed by several particles. The eigenmode decomposition draws its

strength from the fact that it provides a natural framework for describing plasmon-mode hybridization. We provide a proof of concept of this eigenvector expansion (EVE) method by calculating EEL and optical extinction spectra of isolated and coupled silver nanosquares, the results of which are validated by comparison with those obtained from the full DDA.

II. DESCRIPTION OF THE METHOD

This section is divided in two parts: the DDA is first reviewed and the EVE formalism is introduced afterwards.

A. Discrete-dipole approximation

In the DDA,[33] a particle is described as a set of N interacting polarizable elements arranged on a cubic lattice. We work in the frequency domain ω, and thus, an overall $\exp(-i\omega t)$ time dependence is assumed. The dipole moment $\mathbf{p}_j$ of the element located at $\mathbf{r}_j$ is proportional to the local field at this position:

$$\mathbf{p}_j \equiv \mathbf{p}(\mathbf{r}_j) = \alpha_j \mathbf{E}_j^{\mathrm{loc}}, \tag{1}$$

where α_j is the polarizability of the element, which is related to the dielectric function ε_j of the material via the Clausius-Mossotti relation[35]

$$\alpha_j = \frac{3V}{4}\frac{\varepsilon_j - 1}{\varepsilon_j + 2}. \tag{2}$$

Here, V is the volume of the element. The local field at $\mathbf{r}_j$ is given by the superposition of the applied external field and the sum of the scattered fields coming from the other dipoles, so that Eq. (1) becomes

$$\mathbf{p}_j = \alpha_j \left[\mathbf{E}_j^{\mathrm{ext}} + \sum_{n\neq j}^{N} \mathbf{T}_{jn}\mathbf{p}_n \right], \tag{3}$$

where $\mathbf{T}_{jn}$ is the dipole-dipole interaction matrix, which we can write as

$$\mathbf{T}_{jn} = \frac{e^{ikr_{jn}}}{r_{jn}}\left[k^2\left(\mathbf{I}_{3x3} - \frac{\mathbf{r}_{jn}\otimes\mathbf{r}_{jn}}{r_{jn}^2}\right) - \frac{1-ikr_{jn}}{r_{jn}^2}\left(\mathbf{I}_{3x3} - 3\frac{\mathbf{r}_{jn}\otimes\mathbf{r}_{jn}}{r_{jn}^2}\right)\right], \tag{4}$$

$k = \frac{2\pi}{\lambda}$, $\mathbf{r}_{jn} = \mathbf{r}_j - \mathbf{r}_n$, $r_{jn} = |\mathbf{r}_{jn}|$, and $\otimes$ is the dyadic product.[35] Traditionally, the $3N \times 3N$ system of equations (3) is solved numerically via either direct inversion (DI) or iterative techniques (IT), such as conjugate gradient, for a given external field.[34]

To get the optical response of the nanoparticles, the external field is set to a plane wave

$$\mathbf{E}_j^{\mathrm{ext}} = \mathbf{E}_0 e^{i\mathbf{k}.\mathbf{r}_j}, \tag{5}$$

and the extinction cross section is then given by[33]

$$C_{\mathrm{ext}}(\omega) = \frac{4\pi k}{|\mathbf{E}_0|^2}\sum_{j=1}^{N}\mathrm{Im}\left\{\mathbf{E}_j^{\mathrm{ext},*}\cdot\mathbf{p}_j\right\}. \tag{6}$$

Likewise, for a beam of fast electrons traveling along the z direction with velocity v and impact parameter $\mathbf{r}_q$ in the x-y plane, the external field supplied by the electron (i.e., the ω component of this field) has the following components:[34]

$$\begin{aligned}
\mathrm{E}_{j,x}^{\mathrm{ext}} &= \frac{-e\omega}{2\pi\varepsilon_0 v^2\gamma} e^{i\omega\frac{z_j}{v}} \frac{d_{j,x}}{d_j}\mathrm{K}_1\left(\frac{\omega d_j}{\gamma v}\right),\\
\mathrm{E}_{j,y}^{\mathrm{ext}} &= \frac{-e\omega}{2\pi\varepsilon_0 v^2\gamma} e^{i\omega\frac{z_j}{v}} \frac{d_{j,y}}{d_j}\mathrm{K}_1\left(\frac{\omega d_j}{\gamma v}\right),\\
\mathrm{E}_{j,z}^{\mathrm{ext}} &= -\frac{-e\omega}{2\pi\varepsilon_0 v^2\gamma^2} e^{i\omega\frac{z_j}{v}} i\mathrm{K}_0\left(\frac{\omega d_j}{\gamma v}\right),
\end{aligned} \tag{7}$$

where e is the elementary charge, $\mathbf{d}_j = \mathbf{r}_j - \mathbf{r}_q$, $\gamma = \sqrt{1-(\frac{v}{c})^2}$, and K_m is the modified Bessel function of order m. The loss probability reduces to[34]

$$\Gamma_{\mathrm{loss}}(\omega) = \frac{1}{\pi\hbar^2}\sum_{j=1}^{N}\mathrm{Im}\left\{\mathbf{E}_j^{\mathrm{ext},*}\cdot\mathbf{p}_j\right\}. \tag{8}$$

We use Eqs. (6) and (8) to render the spectra shown in the following.

B. Eigenvector expansion method

The main idea of the EVE method is to use a set of eigenvectors as a basis to expand the physical quantities instead of directly solving Eq. (3). The choice of these eigenvectors is then at the core of EVE because it conditions the convergence of the method. The reason why we introduce this approach is that it leads to an efficient way to calculate the response properties of coupled metallic nanoparticles compared with standard DDA, as discussed hereafter.

Let us define the propagator matrix $\mathbf{M}$ of a particle as

$$\mathbf{M} = \begin{bmatrix} \frac{1}{\alpha_1}\mathbf{I}_{3x3} & \cdots & -\mathbf{T}_{1N} \\ \vdots & \ddots & \vdots \\ -\mathbf{T}_{N1} & \cdots & \frac{1}{\alpha_N}\mathbf{I}_{3x3} \end{bmatrix}, \tag{9}$$

and rewrite Eq. (3) in the form

$$\mathbf{M}|\mathbf{P}\rangle = |\mathbf{E}^{\mathrm{ext}}\rangle, \tag{10}$$

where $|\mathbf{E}^{\mathrm{ext}}\rangle$ and $|\mathbf{P}\rangle$ are vectors of dimension $3N$ that contain the applied field and the dipole moment for each discretization element of the particle. Let now $|\mathbf{q}_l\rangle$ be an eigenvector of $\mathbf{Q}$ (i.e., $\mathbf{Q}|\mathbf{q}_l\rangle = q_l|\mathbf{q}_l\rangle$), the "geometric matrix" defined as the electrostatic limit ($kr \to 0$) of $\mathbf{M}$ with null trace

$$\mathbf{Q} = \mathbf{M}|_{kr\to 0} - \begin{bmatrix} \frac{1}{\alpha_1}\mathbf{I}_{3x3} & \cdots & 0 \\ \vdots & \ddots & \vdots \\ 0 & \cdots & \frac{1}{\alpha_N}\mathbf{I}_{3x3} \end{bmatrix}. \tag{11}$$

Because this matrix is symmetric, one can use these vectors as a complete set of orthonormal basis functions and write

$$|\mathbf{E}^{\mathrm{ext}}\rangle = \sum_{l=1}^{l_{\max}} e_l|\mathbf{q}_l\rangle, \tag{12}$$

$$|\mathbf{P}\rangle = \sum_{l=1}^{l_{\max}} p_l|\mathbf{q}_l\rangle. \tag{13}$$

Inserting these expressions in (10) and projecting on $\langle \mathbf{q}_l |$, we obtain

$$\sum_{l'=1}^{l_{\max}} m_{ll'} p_{l'} = e_l, \tag{14}$$

where $m_{ll'} = \langle \mathbf{q}_l | \mathbf{M} | \mathbf{q}_{l'} \rangle$. Because the eigenvectors form a complete basis set, the expansion coefficient p_l can then be calculated from this equation noticing that $e_l = \langle \mathbf{q}_l | \mathbf{E}^{\text{ext}} \rangle$. One could have thought to use the eigenvectors of the propagator matrix but, as it is not Hermitian, they do not form a complete set of orthonormal functions and hence are not appropriate to our problem. Furthermore, it is numerically more efficient to diagonalize a real symmetric matrix (i.e., $\mathbf{Q}$) than a complex one.

At this point, two main advantages of EVE can already be mentioned:

(1) It is possible to truncate the order of expansion $l_{\max}$ to a number that is much smaller than $3N$ (for instance, in the following we use $l_{\max} = 3$ for a system of $N = 3600$ dipoles). To this purpose, one needs to choose carefully the $l_{\max}$ eigenvectors that will be used in Eq. (13). In this paper, they are the ones that give the largest values of $|e_l/q_l|$. Although this criterion may seem somewhat arbitrary, the physical justification is that it represents the probability for the ω component of the external field to excite the eigenmode, taking into account the symmetry properties of the field and the particle (i.e., e_l) and some kind of "intrinsic polarizability" of the eigenmode (i.e., $1/q_l$). The criterion can then be seen as a way to choose the eigenvectors that are the most excitable by a given external field.

(2) It can be easily generalized to clusters of interacting particles. Indeed, each particle μ of a cluster can be described by its own propagator matrix $\mathbf{M}^\mu$, so that Eq. (10) becomes

$$\mathbf{M}^\mu |\mathbf{P}^\mu\rangle = |\mathbf{E}^{\text{ext},\mu}\rangle + \sum_{\nu \neq \mu} \mathbf{\Lambda}^{\mu\nu} |\mathbf{P}^\nu\rangle, \tag{15}$$

with $\Lambda^{\mu\nu}$ given by

$$\mathbf{\Lambda}^{\mu\nu} = \begin{bmatrix} -\mathbf{T}_{11}^{\mu\nu} & \cdots & -\mathbf{T}_{1N_\nu}^{\mu\nu} \\ \vdots & \ddots & \vdots \\ -\mathbf{T}_{N_\mu 1}^{\mu\nu} & \cdots & -\mathbf{T}_{N_\mu N_\nu}^{\mu\nu} \end{bmatrix}, \tag{16}$$

where $\mathbf{T}_{ij}^{\mu\nu}$ is the dipole-dipole interaction matrix that connects the dipole component j of particle ν to the dipole component i of particle μ. Using the same expansion as in Eqs. (12) and (13) and projecting Eq. (15) on $\langle \mathbf{q}_l^\mu |$, the following system of equations is obtained:

$$\sum_{l'=1}^{l_{\max}} m_{ll'}^\mu p_{ll'}^\mu = e_l^\mu + \sum_{\nu \neq \mu} \sum_{l''=1}^{l_{\max}} \lambda_{ll''}^{\mu\nu} p_{l''}^\nu, \tag{17}$$

where $m_{ll'}^\mu = \langle \mathbf{q}_l^\mu | \mathbf{M}^\mu | \mathbf{q}_{l'}^\mu \rangle$ and $\lambda_{ll''}^{\mu\nu} = \langle \mathbf{q}_l^\mu | \Lambda^{\mu\nu} | \mathbf{q}_{l''}^\nu \rangle$ is an interparticle coupling coefficient. This system can be solved with standard iterative techniques once all the eigenvalues and eigenvectors of each particle are known.

The formulation of EVE for several particles has some advantages compared with standard DDA. First, the geometric matrix (11) of a particle depends only on the relative positions of the dipoles and is completely independent of their absolute positions and orientations. The geometric matrix is also frequency independent and its diagonalization has to be made one time for all the spectrum and, once this step is completed, the resulting eigenvectors can be stored and reutilized in any further calculations (for which particles can be translated or rotated). These ones are chosen as in the isolated particle case: for each particle μ, only the first $l_{\max}$ eigenvectors that yield the largest values of $|e_l^\mu/q_l^\mu|$ are retained.

Additionally, the algorithm is less computationally demanding than traditional DDA approaches. For example, let us consider a cluster of N_{part} identical particles described by N_{dip} dipoles. The computational demand scales as $(N_{\text{part}} N_{\text{dip}})^3$ for direct inversion, whereas it scales as $N_{\text{it}}(N_{\text{part}} N_{\text{dip}})^2$ for iterative techniques (for instance, conjugate gradient), where N_{it} is the number of iterations needed to achieve convergence. In contrast, the EVE algorithm consists of two different parts: inversion of the propagator matrix, which scales as N_{dip}^3, and calculation of coupling terms, which requires $l_{\max}^2 (N_{\text{part}} N_{\text{dip}})^2$ operations, where $l_{\max}$ is the expansion order. The complexity of the EVE method is then roughly given by $N_{\text{dip}}^3 + l_{\max}^2 (N_{\text{part}} N_{\text{dip}})^2$, and the dominant term depends on the size of the cluster and the expansion order. For clusters formed by many particles, we have ratios $\gamma^{\text{EVE/DI}} \approx l_{\max}^2 / N_{\text{part}} N_{\text{dip}}$ between EVE and direct inversion and $\gamma^{\text{EVE/IT}} \approx l_{\max}^2 / N_{\text{it}}$ between EVE and iterative techniques. Obviously, these ratios can be substantially lower than 1 depending on the choice of parameters.

Notice that although the propagator matrix is frequency dependent in general electrodynamic problems, this is not the case when one deals with small homogeneous particles ($\alpha_i = \alpha$, $i = 1, \ldots, N$) within the electrostatic limit ($kr \to 0$). In this case, Eq. (14) reduces to $m_l p_l = e_l (l = 1, \ldots, l_{\max})$ with $m_l = q_l + 1/\alpha$, hence decreasing the computational cost of the EVE method.

III. RESULTS AND DISCUSSION

We present here testing results for the EVE method applied to isolated and coupled flat silver square nanoparticles of 24-nm side length (in the x and y directions) and 6-nm height (in the z direction). An individual particle is described by 3600 dipoles, and because of its small size compared with the light wavelength, we work within the electrostatic limit. The dielectric function of silver is taken from tabulated data.[36]

A. Isolated silver square

As a first example, we compare the optical extinction spectra of an isolated silver square excited by a plane wave traveling along z and polarized along y that are obtained by nonretarded EVE (nr-EVE) to the ones given by retarded and nonretarded DDA (r-DDA and nr-DDA, respectively) calculations. The results in Fig. 1(a) show that there is a strong and sharp resonance at 2.13 eV and a small bump at 2.93 eV. The position of the resonances matching with both retarded and nonretarded DDA reveals that the electrostatic approximation used with EVE is valid in this context. From Fig. 1(a), one can see that only one eigenvector is sufficient to get the correct position of the peaks and that the intensity

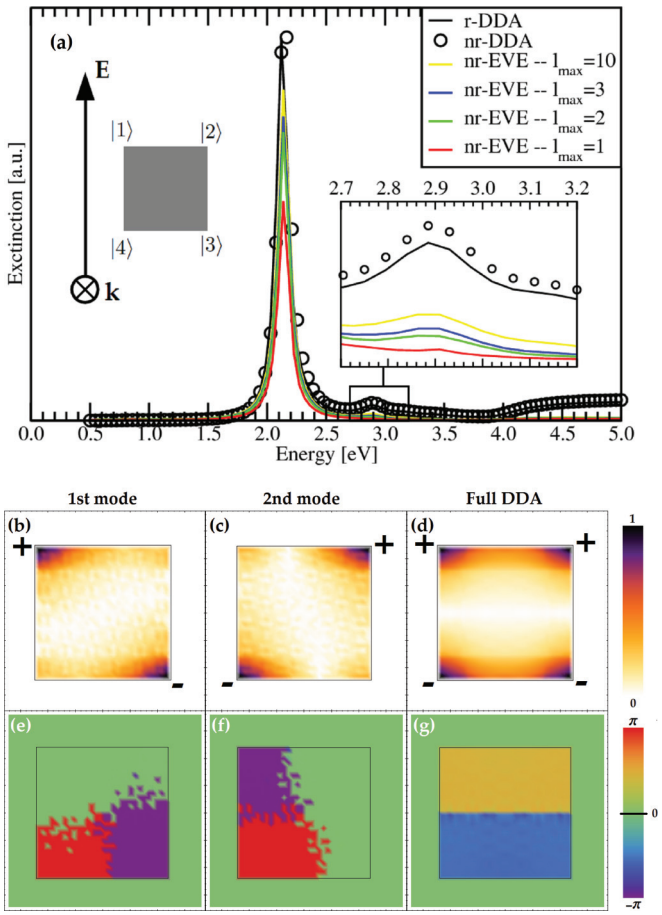

FIG. 1. (Color online) (a) Extinction spectra of an isolated silver square calculated with retarded (black curve) and nonretarded DDA (black circle), as well as nonretarded EVE with 1 (red curve), 2 (green curve), 3 (blue curve), and 10 (yellow curve) eigenvectors. The particle has side length of 24 nm (in the x and y directions) and 6 nm in height (in the z direction). (b)–(g) Normalized modulus [(b), (c)] and phase [(e), (f)] maps of the charge integrated along the z direction (z-IC) for the first two eigenmodes and full DDA calculation [(d), (g)] of an isolated silver square excited by a plane wave of 2.13 eV. The integration radius is $a = 4$ nm. Charge signs are added to help visualizing the modes.

of the resonances rises as the expansion order is increased. Furthermore, the contribution of a given term of the expansion to the total intensity becomes smaller and smaller as its order is high, a behavior that is expected in any convergent expansion method. If the intensity of the 2.13-eV resonance converges quite rapidly with the expansion order, this is not so true for the 2.93-eV resonance as can be seen from the zoom in Fig. 1(a). This behavior is due to the more complicated geometry of this mode and will be explained hereafter when EEL calculations will be performed. The fact remains that, in the following, we will always use a basis set of three eigenvectors as it is a good compromise between accuracy and calculation time.

These eigenvectors can be seen as some "geometrical eigenmodes" of the particles and they are chosen depending on how they will interact with the external field. A way to get a representation of these eigenmodes is to plot the modulus (the intensity) and the phase [the signs which are opposite (even) for phase delay of π (2π) between two points] of the charge integrated along the z direction. Indeed, because the particle is too thin in this direction for retardation to occur, there will be no phase change from one side to the other. The z-direction integrated charge (z-IC) at frequency ω is defined as

$$Q^z(x,y;\omega) = \int_0^h q(x,y,z;\omega)dz, \tag{18}$$

with h being the thickness of the particle. The charge $q(\mathbf{r};\omega)$ at a point $\mathbf{r} = (x,y,z)$ can be obtained by integrating the charge density in a volume V' around this point, i.e., $q(\mathbf{r};\omega) = \int_{V'} \rho(\mathbf{r}';\omega)dV'$, where the charge density is related to the polarization through $\rho(\mathbf{r};\omega) = -\nabla \cdot \mathbf{P}(\mathbf{r};\omega)$.[35] In the frame of DDA, if one takes V' as a spherical volume of radius a, Eq. (18) becomes

$$Q^z(x_j,y_j;\omega) = \frac{h}{T}\sum_{t=1}^{T} q(x_j,y_j,z_t;\omega), \tag{19}$$

with $q(\mathbf{r}_j;\omega) = -\frac{4\pi a^3}{3N'V}\sum_{n=1}^{N'} \nabla_n \cdot \mathbf{p}_n$, T and N' being the number of dipoles along the thickness of the particle and in the volume V', respectively.

Figures 1(b), 1(c), 1(e), and 1(f) show the normalized modulus and the phase of the z-IC for the first two eigenmodes of the silver square at 2.13 eV calculated for a radius of $a = 4$ nm. They are degenerated and correspond to modes where two opposite corners with respect to a diagonal are excited with the same intensities but opposite charges (due to the π phase delay). The third mode (not shown) also has its maximum intensity on two opposite corners with the same symmetry as the first mode but it has more charge oscillations in the central part. This feature makes it a higher-eigenvalue mode and it is then less contributing in the expansion. As stated by Eq. (13), the dipole moments are formed by a linear combination of the eigenmodes. It results in a dipolar mode aligned with the polarization vector (along the y axis) for which each corner has the same intensity but with opposite sign in the upper and lower corners as shown in Figs. 1(d) and 1(g).

It is interesting to perform group-theory analysis to get information on the symmetries of the modes supported by the square nanoparticle.[37] For this, let us consider it to be two dimensional (a good approximation due to the small thickness of the particle) so that the point group is C_{4v}. In analogy with the tight-binding model used in solid-state physics,[38] it is possible to describe a plasmon mode as a combination of interacting localized corner states. If $|n\rangle$ is the state localized at corner n [see inset of Fig. 1(a)], a plasmon mode can be written as $|\psi\rangle = \sum_{n=1}^{4} c_n|n\rangle$. The representation of C_{4v} in the basis set $\{|n\rangle\}$ has the following irreducible representations decomposition: $\Gamma^{(n)} = \mathrm{A}_1 \oplus \mathrm{B}_2 \oplus \mathrm{E}$ (see Appendix A). To each of these irreducible representations correspond the following linear combinations of the basis functions:

$$\mathrm{A}_1 \Rightarrow |\psi^{\mathrm{A}_1}\rangle = \tfrac{1}{2}[|1\rangle + |2\rangle + |3\rangle + |4\rangle], \tag{20}$$

$$\mathrm{B}_2 \Rightarrow |\psi^{\mathrm{B}_2}\rangle = \tfrac{1}{2}[|1\rangle - |2\rangle + |3\rangle - |4\rangle], \tag{21}$$

$$\mathrm{E} \Rightarrow \begin{cases} |\psi_1^{\mathrm{E}}\rangle = \frac{1}{\sqrt{2}} & [|1\rangle - |3\rangle], \\ |\psi_2^{\mathrm{E}}\rangle = \frac{1}{\sqrt{2}} & [|2\rangle - |4\rangle]. \end{cases} \tag{22}$$

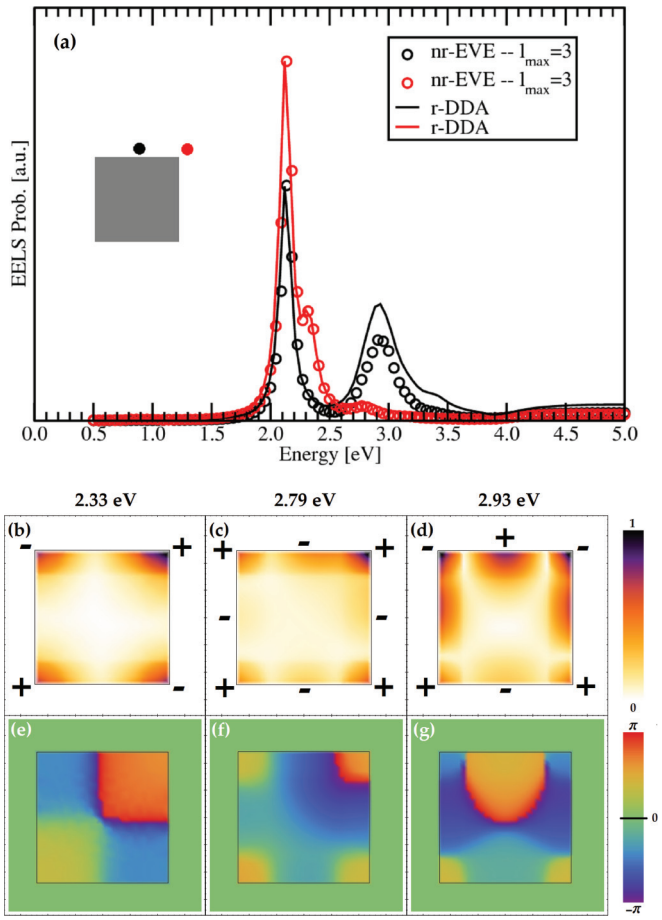

FIG. 2. (Color online) (a) EEL spectra of an isolated silver square calculated with retarded DDA (solid curves) and nonretarded EVE with three eigenvectors (circles) for the two representative impact parameters (in black and red). The particle has side length of 24 nm and 6 nm in height. (b)–(g) Normalized modulus and phase maps of the z-IC of the 2.33-eV [(b), (e)], 2.79-eV [(c), (f)], and 2.93-eV [(d), (g)] modes calculated by nr-EVE. The integration radius is $a = 4$ nm. Charge signs are added to help visualizing the modes.

The first one is a one-dimensional totally symmetric combination, the second is one dimensional with a quadrupolar symmetry where corners have the same intensity but alternate in sign, and the last one is a two-dimensional combination with dipolar symmetry along the diagonals. Comparing these results to the $l = 1$ and 2 eigenmodes of Fig. 1, it appears that they correspond exactly to $|\psi_1^{\mathrm{E}}\rangle$ and $|\psi_2^{\mathrm{E}}\rangle$ with $|n\rangle$ being basis functions made of a localized "+" charge and that the resulting dipolar plasmon mode $|\psi_d\rangle$ is given by their sum: $|\psi_d\rangle = |\psi_1^{\mathrm{E}}\rangle + |\psi_2^{\mathrm{E}}\rangle$.

We are now turning our attention to EEL spectra of the same particle [Fig. 2(a)]. Full r-DDA calculations have been performed for an electron passing near the middle of an edge (black curve) or near a corner (red curve). Because of the localized nature of the excitation, spectra have additional features that correspond to higher-order modes that can not be excited optically. Apart from the dipolar mode present at 2.13 eV for both impact parameters, there are also resonances at 2.33 and 2.79 eV when the electron passes near the corner. For an electron passing near the middle of an edge, one can see that the peak at 2.93 eV is much more intense than in the extinction spectrum. Computing the z-IC gives the signature of these modes [Figs. 2(b)–2(g)] and they are identified as being the quadrupolar [Figs. 2(b) and 2(e)], octupolar [Figs. 2(c) and 2(f)], and edge [Figs. 2(d) and 2(g)] modes, respectively.

The same calculations have been made using the nr-EVE method with three eigenvectors (black and red circles) that are not the same as the ones composing the dipolar resonance of the extinction spectra, their selection depending on a different external field. For instance, the first eigenmode at 2.33 eV has quadrupolar symmetry that corresponds to a $|\psi^{\mathrm{B}_2}\rangle$ state where the basis function $|n\rangle$ is made of localized "+" charge and the next two eigenvectors have dipolar symmetry and higher-order quadrupolar symmetry, respectively (see Fig. 7). As for the optical spectra, peak positions are identical with both techniques but, as previously stated, the peaks' intensities are not properly evaluated because of the truncation of the expansion. Therefore, spectra have been renormalized with a multiplication factor such that the maxima of the spectra are in coincidence in the figure. It appears that if the 2.33-eV modes have also the same intensity, this is not the case for the 2.79- and 2.93-eV modes which are significatively less intense in nr-EVE. This can be explained by the fact that the geometry of these modes is more complicated and, as a consequence, intensity is distributed among more eigenmodes (see Figs. 8 and 9).

B. Silver square dimer

Coupled particles support more complex modes and this section will deal with dimers of silver square coupled in two ways: corner to corner and edge to edge. Calculations have been performed using the nr-EVE method with three eigenvectors. They can be compared to r-DDA results gathered in Appendix C. It is interesting to note that, with these computational parameters, the complexity ratios are estimated around $\gamma^{\mathrm{EVE/DI}} \approx \frac{1}{800}$ and $\gamma^{\mathrm{EVE/IT}} \approx \frac{1}{6}$ with an average of $N_{\mathrm{it}} = 60$ over a full spectrum.

The corner-to-corner case is considered first and the results for a 2-nm gap are shown in Fig. 3(a) where the EEL curves are calculated for impact parameters of corresponding color. When the electron is passing in the gap between the particles (black case), two strong peaks are observed at 2.21 and 2.40 eV which correspond to symmetric dipolar and quadrupolar modes, respectively, as can be seen from the z-IC maps [Figs. 3(c), 3(d), 3(f), and 3(g)]. Both of them are dark modes because of the vanishing dipole moment carried by the structure and do not appear in the optical spectrum [blue circles in Fig. 3(a)]. For an impact parameter situated near a corner on the dimer axis but not in the gap (red case), the EEL spectrum has a peak at 1.99 eV which is an antisymmetric dipolar mode [Figs. 3(b) and 3(e)] that one can observe in the extinction spectrum. There is also a peak at 2.21 eV corresponding to the same symmetric dipolar mode mentioned before but no antisymmetric quadrupolar mode is observed. For a trajectory that is near a corner that is not on the dimer axis (green case), no coupling occurs and the spectrum is essentially the same as the one of an isolated square. Indeed, particles interact with one another if their near fields overlap, i.e., if they are localized in the gap between the particles. In the green case, the near field is localized around the excited corner and its opposite so

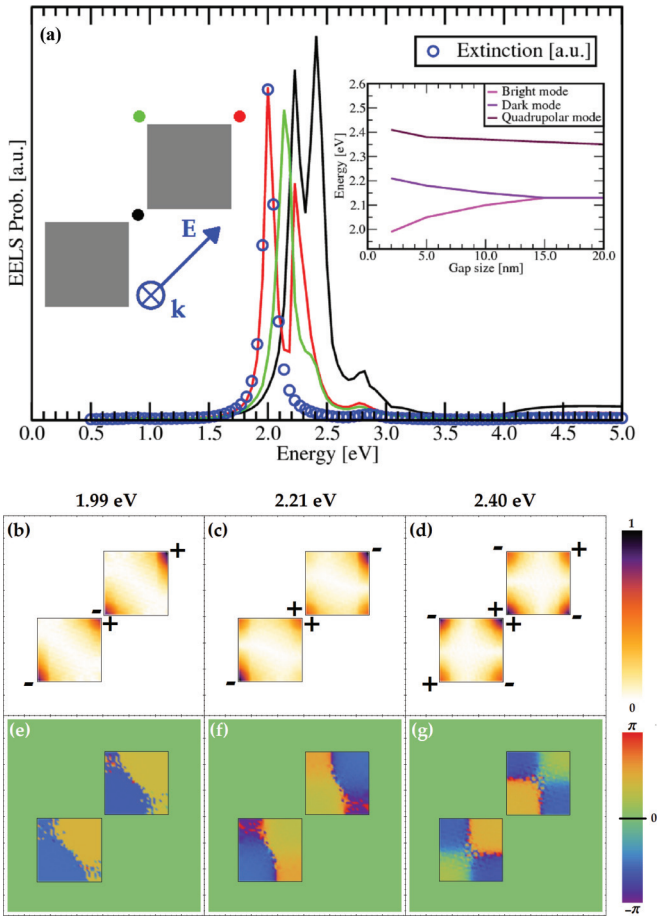

FIG. 3. (Color online) (a) Extinction (blue circles) and EEL (black and red curves) spectra of a corner-to-corner silver dimer with 2-nm interparticle gap. The particles have side length of 24 nm and 6 nm in height. Inset: effect of the interparticle distance on the position of the excited modes. (b)–(g) Normalized modulus and phase maps of the z-IC of the 1.99-eV [(b), (e)], 2.21-eV [(c), (f)], and 2.40-eV [(d), (g)] modes calculated by nr-EVE. The integration radius is $a = 4$ nm. Charge signs are added to help visualizing the modes.

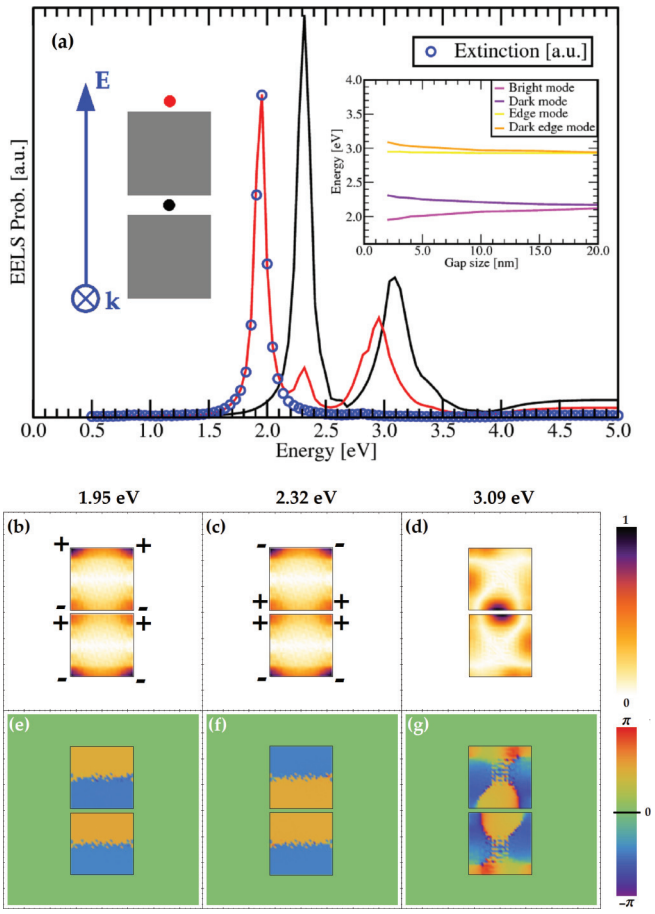

FIG. 4. (Color online) (a) Extinction (blue circles) and EEL (black and red curves) spectra of an edge-to-edge silver dimer with 2-nm interparticle gap. The particles have side length of 24 nm and 6 nm in height. Inset: effect of the interparticle distance on the position of the excited modes. (b)–(g) Normalized modulus and phase maps of the z-IC of the 1.95-eV [(b), (e)], 2.32 eV [(c), (f)], and 3.09 eV [(d), (g)] modes calculated by nr-EVE. The integration radius is $a = 4$ nm. Charge signs are added to help visualizing the modes.

that there is no field in the gap to make coupling possible. On the other hand, for the black and red trajectories, the near fields are localized on the corners along the dimer axis (thus in the gap) and interaction can occur. The effect of the interparticle distance has also been investigated [inset of Fig. 3(a)]. Two observations can be made: (1) interaction between dipolar modes occurs for larger gap than for quadrupolar modes and the shifts are greater, and (2) symmetric (dark) modes shift to higher energies while antisymmetric (bright) modes shift to lower energies. These observations can be explained by the larger spatial extent of the near field of a dipolar mode compared to the one of a dark mode. Because of this, the overlapping between near fields of neighboring dipolar modes of the particles can occur at larger distances and it decreases as the gap becomes larger and larger until there is no overlap anymore.

The same calculations have been performed for an edge-to-edge silver dimer with a 2-nm gap. The results are gathered in Fig. 4. Two impact parameters passing through the dimer axis have been considered: one in the gap (black case) and one in the outside region (red case). In the first case, one can distinguish two peaks at 2.32 and 3.09 eV for which the z-IC maps show that they are symmetric dipolar and edge modes, respectively. For the other trajectory, three resonances appear: an antisymmetric dipolar mode at 1.95 eV, a symmetric dipolar mode at 2.32 eV, and an edge mode at 2.93 eV. This last mode is equivalent to the one excited in an isolated square. Indeed, the position of this peak does not change with the gap size as can be seen in the inset of Fig. 4(a). That means there is no coupling between the particles and only the nearest particle is excited with this mode. Compared to the corner-to-corner case, the same conclusions can be made except that the interaction length between the dipolar modes is greater when particles are in an edge-to-edge configuration and that the shifts are also higher in this case. This is due to the fact that interaction takes place in two corners instead of one as in the corner-to-corner case.

C. Silver square quadrumers

Because the EVE method is to be more efficient for systems with many particles, it is now applied to quadrumers of silver

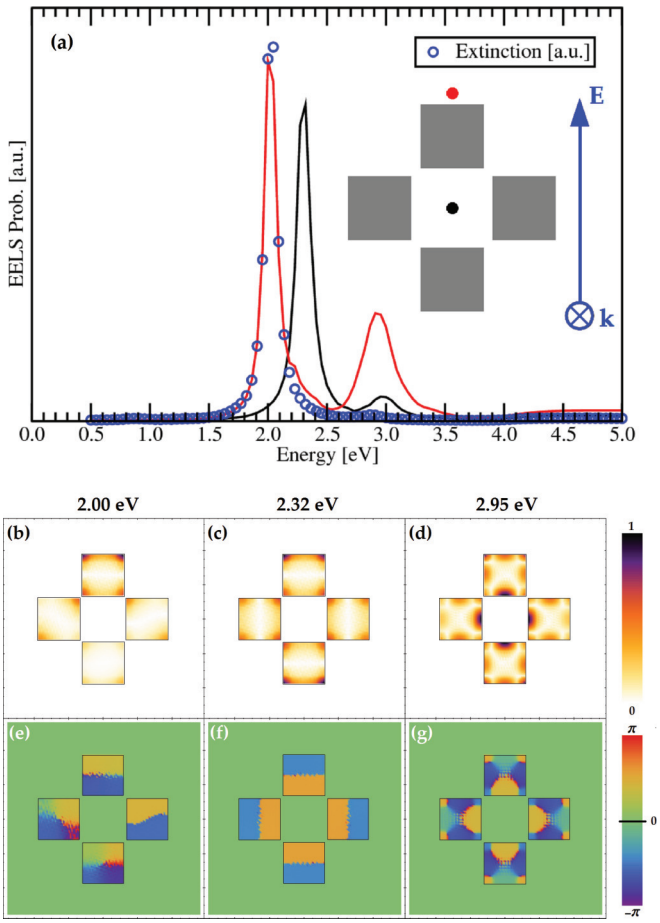

FIG. 5. (Color online) (a) Extinction (blue circles) and EEL (black and red curves) spectra of a corner-to-corner silver quadrumer with 2-nm interparticle gap. The particles have side length of 24 nm and 6 nm in height. (b)–(g) Normalized modulus and phase maps of the z-IC of the 2.00-eV [(b), (e)], 2.32-eV [(c), (f)], and 2.95 eV [(d), (g)] modes calculated by nr-EVE. The integration radius is $a = 4$ nm.

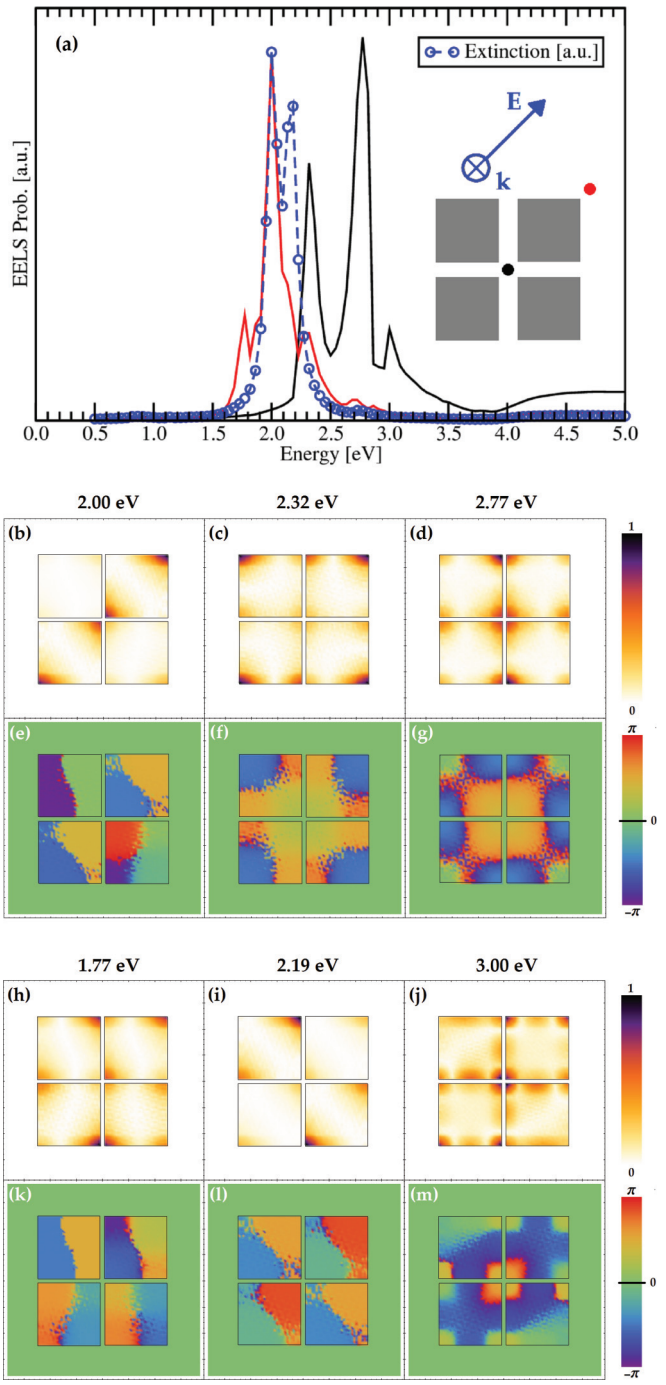

FIG. 6. (Color online) (a) Extinction (blue circles) and EEL (black and red curves) spectra of an edge-to-edge silver quadrumer with 2-nm interparticle gap. The particles have side length of 24 nm and 6 nm in height. (b)–(m) Normalized modulus and phase maps of the z-IC of the 2.00-eV [(b), (e)], 2.32-eV [(c), (f)], 2.77-eV [(d), (g)], 1.77-eV [(h), (k)], 2.19-eV [(i), (l)], and 3.00-eV [(j), (m)] modes calculated by nr-EVE. The integration radius is $a = 4$ nm.

squares to demonstrate its ability. The complexity ratios can be estimated around $\gamma^{\mathrm{EVE/DI}} \approx \frac{1}{1600}$ and $\gamma^{\mathrm{EVE/IT}} \approx \frac{1}{10}$ with an average of $N_{\mathrm{it}} = 100$ over a full spectrum.. As for the dimers, two geometries are considered: corner to corner and edge to edge. In both cases, the particles are arranged on a square lattice with a 2-nm interparticle distance. To keep the analysis as simple as possible, only two electron trajectories have been studied and compared to extinction spectra. One is passing at the of center of symmetry of the quadrumers and the second is taken outside the quadrumers and is contained in a mirror plane of the structure.

Figure 5(a) shows the extinction and EEL spectra of the corner-to-corner quadrumer. It appears that one strong resonance is observed at 2.32 eV and a smaller one at 2.95 eV for an impact parameter positioned at the center of symmetry (black curve). On the other hand, an intense peak is identified at 2.00 eV and the 2.95-eV resonance becomes more pronounced when the electron is passing near an edge in the outside region of the quadrumer (red curve). From the z-IC maps [Figs. 5(b)–5(g)], it is clear that the 2.00-eV mode is an antisymmetric dipolar mode [Figs. 5(b) and 5(e)], whereas the 2.32- and 2.95-eV ones are totally symmetric combinations of dipolar [Figs. 5(c) and 5(f)] and edge [Figs. 5(d) and 5(g)] modes, respectively. The former is bright and the latter are dark as confirmed by the extinction spectrum [blue circles in Fig. 5(a)].

Considering now the edge-to-edge case (Fig. 6), EEL calculations reveal more complex patterns, but three modes are dominating the spectra. The first one at 2.00 eV is excited when the electron is passing near one of the outside corners of the structure (red curve) and correspond to an antisymmetric dipolar mode that is the same as the one observed in the dimer case. Indeed, the z-IC map [Figs. 6(b) and 6(e)] shows that the upper left and lower right nanoparticles are hardly excited. The other two intense modes appear at 2.32 and 2.77 eV for the trajectory passing through the center of symmetry (black curve). They are identified as symmetric combinations of dipolar and quadrupolar modes [Figs. 6(c) and 6(f) and 6(d) and 6(g), respectively] and hence are dark. The extinction spectrum [blue circles in Fig. 6(a)] corroborates these results but one can observe an additional feature at 2.19 eV. This is a mode for which the upper left and lower right nanoparticles support in-phase dipolar resonances aligned with the polarization while the other two squares are not excited [the exact complementary situation observed at 2.00 eV, see Figs. 6(i) and 6(l)]. It barely appears in the EEL spectrum (just a small bump in the red curve) because of the symmetry break introduced in the system by the presence of the electron. Finally, it worth noting the presence of two less intense dark modes at 1.77 and 3.00 eV. The latter is a symmetric combination of octupolar modes [Figs. 6(j) and 6(m)], whereas the former is made of dipolar modes with a π-phase delay between the upper and the lower ones [Figs. 6(h) and 6(k)].

IV. CONCLUSIONS

We have developed an approach to compute optical extinction and electron energy-loss spectra of isolated and coupled metallic nanoparticles that is based on an efficient modification of the DDA. It consists in computing eigenvectors of a geometric matrix describing the particles instead of directly solving the full system of equations. These eigenvectors are then used as a truncatable basis to expand the physical quantities entering the DDA formalism. We have shown that only a few eigenmodes are needed to obtain accurate optical extinction and electron energy-loss spectra of systems made of isolated and coupled flat silver squares. A correspondence between the eigenvectors and the irreducible representations of the symmetry group of the square has been made based upon group theory. With these results, we demonstrate that our approach introduces a significant gain in computational efficiency compared with traditional DDA approaches. Additionally, it provides a natural framework for the numerical study of plasmons of coupled metallic nanoparticles.

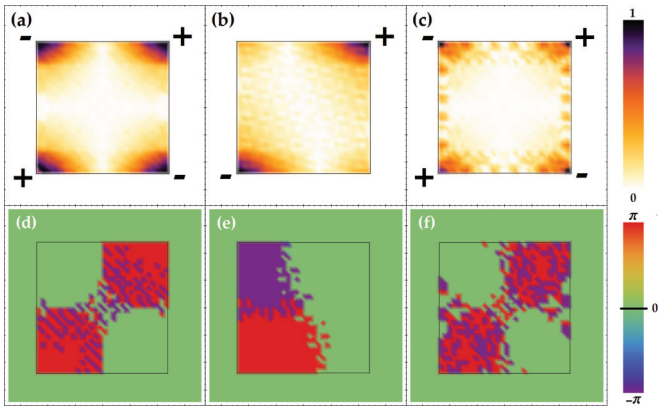

FIG. 7. (Color online) Normalized modulus and phase maps of the z-IC of the first [(a), (d)], second [(b), (e)], and third [(c), (f)] eigenmodes forming the quadrupolar resonance at 2.33 eV of an isolated silver square excited by an electron passing near a corner. The particle has side length of 24 nm and 6 nm in height. The integration radius is $a = 4$ nm. Charge signs are added to help visualizing the modes.

ACKNOWLEDGMENTS

S.-O.G. is supported by the Belgian fund F.R.I.A. This research used resources of the "Plateforme Technologique de Calcul Intensif (PTCI)" (http://www.ptci.unamur.be) located at the University of Namur, Belgium, which is supported by the F.R.S.-FNRS. The PTCI is member of the Consortium des Equipements de Calcul Intensif (CECI) (http://www.ceci-hpc.be). F.J.G.A. acknowledges support from the Spanish MEC (MAT2010-14885 and Consolider NanoLight.es) and the European Commission (FP7-ICT-2009-4-248855-N4E).

APPENDIX A: REDUCTION OF $\Gamma^{(n)}$

The character table of C_{4v} is

C_{4v}	E	$2C_4$	C_2	$2\sigma_v$	$2\sigma_d$
A_1	1	1	1	1	1
A_2	1	1	1	−1	−1
B_1	1	−1	1	1	−1
B_2	1	−1	1	−1	1
E	2	0	−2	0	0

We intend to express $\Gamma^{(n)}$ in the form of a direct sum of irreducible representations (i.e., $\Gamma^{(n)} = \sum_{l\oplus} n_l \Gamma^{(l)}$, where $\Gamma^{(l)}$ is an irreducible representation of C_{4v} and n_l the number of times that it appears in the sum). It is given by

$$n_l = \frac{1}{g} \sum_G \chi^{l,*}(G)\chi^n(G), \tag{A1}$$

where g is the number of elements in the group, $\chi^l(G)$ is the character of element G in representation l, and the sum runs over the elements of the group. The characters of the representation in the basis set $\{|n\rangle\}$ are

$$\chi^n(E) = 4, \quad \chi^n(C_4) = 0, \quad \chi^n(C_2) = 0,$$
$$\chi^n(\sigma_v) = 0, \quad \chi^n(\sigma_d) = 2.$$

Using Eq. (A1), we obtain the following numbers:

$$n_{A_1} = 1, \quad n_{A_2} = 0, \quad n_{B_1} = 0,$$
$$n_{B_2} = 1, \quad n_E = 1,$$

and $\Gamma^{(n)} = A_1 \oplus B_2 \oplus E$.

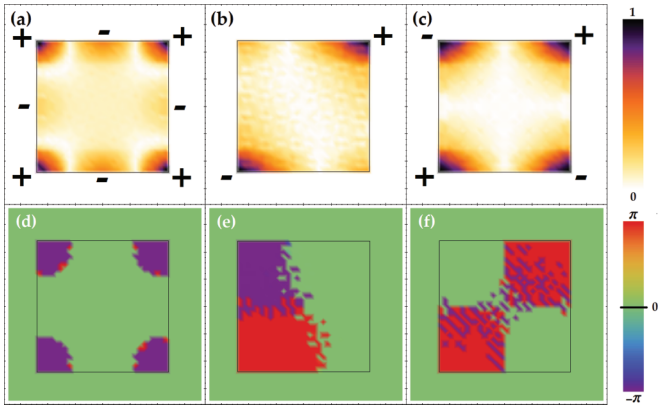

FIG. 8. (Color online) Normalized modulus and phase maps of the z-IC of the first [(a), (d)], second [(b), (e)], and third [(c), (f)] eigenmodes forming the octupolar resonance at 2.79 eV of an isolated silver square excited by an electron passing near a corner. The particle has side length of 24 nm and 6 nm in height. The integration radius is $a = 4$ nm. Charge signs are added to help visualizing the modes.

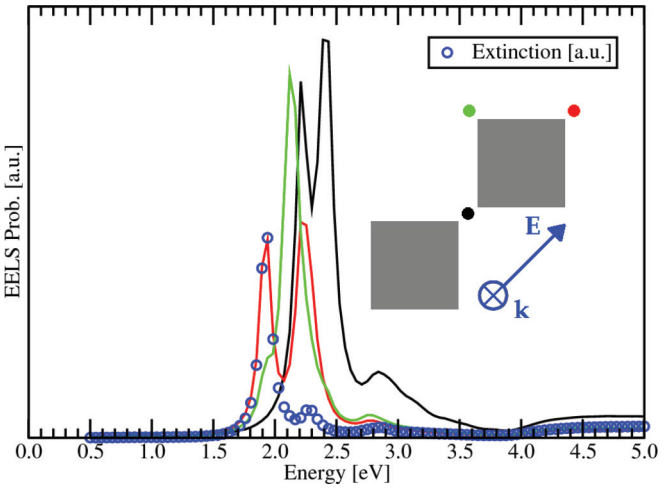

FIG. 10. (Color online) Extinction (blue circles) and EEL (black and red curves) spectra of a corner-to-corner silver dimer with 2-nm interparticle gap calculated with r-DDA. The particles have side length of 24 nm and 6 nm in height.

APPENDIX B: SUPPLEMENTARY INTEGRATED CHARGE MAPS

This appendix gathers maps of the charge integrated along the z direction (z-IC) of the first, second, and third eigenmodes which combined give the quadrupolar (Fig. 7), octupolar (Fig. 8), and edge (Fig. 9) resonances observed in Fig. 2. Because the geometry of these resonances is more complex than in the dipolar case, the peak intensities are distributed among more eigenmodes, explaining why they are not properly reproduced in Fig. 2(a).

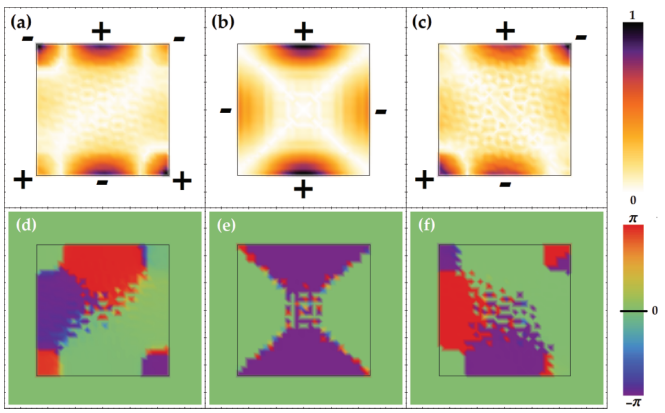

FIG. 9. (Color online) Normalized modulus and phase maps of the z-IC of the first [(a), (d)], second [(b), (e)], and third [(c), (f)] eigenmodes forming the edge resonance at 2.93 eV of an isolated silver square excited by an electron passing near an edge. The particle has side length of 24 nm and 6 nm in height. The integration radius is $a = 4$ nm. Charge signs are added to help visualizing the modes.

APPENDIX C: SUPPLEMENTARY EXTINCTION AND EEL SPECTRA OF SILVER SQUARE DIMERS

Here (see Figs. 10 and 11) are gathered the extinction and EEL spectra of corner-to-corner and edge-to-edge silver square dimers calculated by retarded DDA. The configurations are the same as the ones used in Figs. 3 and 4 so the reader can compare the results obtained by both nr-EVE and r-DDA.

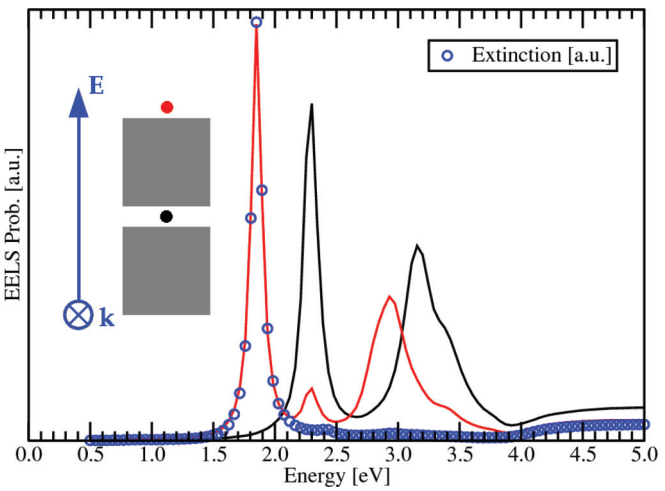

FIG. 11. (Color online) Extinction (blue circles) and EEL (black and red curves) spectra of an edge-to-edge silver dimer with 2-nm interparticle gap calculated with r-DDA. The particles have side length of 24 nm and 6 nm in height.

*luc.henrard@unamur.be

[1] R. Alvarez-Puebla, L. M. Liz-Marzan, and F. J. Garcia de Abajo, J. Phys. Chem. Lett. **1**, 2428 (2010).

[2] B. Paivanranta, H. Merbold, R. Giannini, L. Buchi, S. Gorelick, C. David, J. F. Löffler, T. Feurer, and Y. Ekinci, ACS Nano **5**, 6374 (2011).

[3] C.-D. Chen, S.-F. Cheng, L.-K. Chau, and C. C. Wang, Biosens. Bioelectron. **22**, 926 (2007).

[4] H. A. Atwater and A. Polman, Nat. Mater. **9**, 205 (2010).

[5] D. Lis, Y. Caudano, M. Henry, S. Demoustier-Champagne, E. Ferain, and F. Cecchet, Adv. Opt. Mater. **1**, 244 (2013).

[6] E. Lidorikis, J. Quant. Spectrosc. Radiat. Transfer **113**, 2573 (2012).

[7] N. A. Hatab, C.-H. Hsueh, A. L. Gaddis, S. T. Retterer, J.-H. Li, G. Eres, Z. Zhang, and B. Gu, Nano Lett. **10**, 4952 (2010).

[8] S. Lal, S. Link, and N. J. Halas, Nat. Photonics **1**, 641 (2007).

[9] R. Zia, J. A. Schuller, A. Chandran, and M. L. Brongersma, Mater. Today **9**, 20 (2006).

[10] H. Raether, *Surface Plasmons on Smooth and Rough Surfaces and on Gratings*, 1st ed. (Springer, Berlin, 1988).

[11] K. L. Kelly, E. Coronado, L. L. Zhao, and G. C. Schatz, J. Phys. Chem. B **107**, 668 (2003).

[12] V. Myroshnychenko, J. Rodriguez-Fernandez, I. Pastoriza-Santos, A. M. Funston, C. Novo, P. Mulvaney, L. M. Liz-Marzan, and F. J. Garcia de Abajo, Chem. Soc. Rev. **37**, 1792 (2008).

[13] M. Grzelczak, J. Perez-Juste, P. Mulvaney, and L. M. Liz-Marzan, Chem. Soc. Rev. **37**, 1783 (2008).

[14] E. Hao and G. C. Schatz, J. Chem. Phys. **120**, 357 (2004).

[15] D. W. Brandl, N. A. Mirin, and P. Nordlander, J. Phys. Chem. B **110**, 12302 (2006).

[16] C. L. Haynes, A. D. McFarland, L. Zhao, R. P. Van Duyne, G. C. Schatz, L. Gunnarsson, J. Prikulis, B. Kasemo, and M. Kall, J. Phys. Chem. B **107**, 7337 (2003).

[17] E. Prodan, C. Radloff, N. J. Halas, and P. Nordlander, Science **302**, 419 (2003).

[18] P. Nordlander, C. Oubre, E. Prodan, K. Li, and M. I. Stockman, Nano Lett. **4**, 899 (2004).

[19] M.-W. Chu, V. Myroshnychenko, C. H. Chen, J.-P. Deng, C.-Y. Mou, and F. J. Garcia de Abajo, Nano Lett. **9**, 399 (2009).

[20] A. L. Koh, K. Bao, I. Khan, W. E. Smith, G. Kothleitner, P. Nordlander, S. A. Maier, and D. W. McComb, ACS Nano **3**, 3015 (2009).

[21] J. Nelayah, M. Kociak, O. Stephan, F. J. Garcia de Abajo, M. Tence, L. Henrard, D. Taverna, I. Pastoriza-Santos, L. M. Liz-Marzan, and C. Colliex, Nat. Phys. **3**, 348 (2007).

[22] L. S. Slaughter, Y. Wu, B. A. Willingham, P. Nordlander, and S. Link, ACS Nano **4**, 4657 (2010).

[23] T.-R. Liu, Z.-K. Zhou, C. Jin, and X. Wang, Plasmonics **8**, 885 (2013).

[24] N. Verellen, Y. Sonnefraud, H. Sobhani, F. Hao, V. V. Moshchalkov, P. V. Dorpe, P. Nordlander, and S. A. Maier, Nano Lett. **9**, 1663 (2009).

[25] V. Giannini, Y. Francescato, H. Amrania, C. C. Phillips, and S. A. Maier, Nano Lett. **11**, 2835 (2011).

[26] N. W. Bigelow, A. Vaschillo, J. P. Camden, and D. J. Masiello, ACS Nano **7**, 4511 (2013).

[27] S.-O. Guillaume, N. Geuquet, and L. Henrard, Proc. SPIE **8096**, 80962E (2010).

[28] F. J. Garcia de Abajo and A. Howie, Phys. Rev. B **65**, 115418 (2002).

[29] A. Taflove, *Computational Electrodynamics: The Finite-Difference Time-Domain Method*, 1st ed. (Artech House, Boston, 1995).

[30] C. Matyssek, J. Niegemann, W. Hergert, and K. Busch, Photon. Nanostruct.: Fund. Applicat. **9**, 367 (2011).

[31] M. I. Mishchenko, L. D. Travis, and D. W. Mackowski, J. Quant. Spectrosc. Radiat. Transfer **55**, 535 (1996).

[32] C. Matyssek, V. Schmidt, W. Hergert, and T. Wriedt, Ultramicroscopy **117**, 46 (2012).

[33] B. T. Draine, Astrophys. J. **333**, 848 (1988).

[34] N. Geuquet and L. Henrard, Ultramicroscopy **110**, 1075 (2010).

[35] J. D. Jackson, *Classical Electrodynamics*, 2nd ed. (Wiley, New York, 1975).

[36] E. D. Palik, *Handbook of Optical Constants of Solids*, 1st ed. (Academic, New York, 1985).

[37] W. Zhang, B. Gallinet, and O. J. F. Martin, Phys. Rev. B **81**, 233407 (2010).

[38] V. Myroshnychenko, J. Nelayah, G. Adamo, N. Geuquet, J. Rodriguez-Fernandez, I. Pastoriza-Santos, K. F. MacDonald, L. Henrard, L. M. Liz-Marzán, N. I. Zheludev *et al.*, Nano Lett. **12**, 4172 (2012).